Polyaniline Nanoskein: Synthetic Method, Characterization, and Redox Sensing

Yoochan Hong (ychong1983@kimm.re.kr)
Korea Institute of Machinery and Materials https://orcid.org/0000-0002-6345-9877
Hyun Soo Kim
Korea Institute of Machinery and Materials
Taeha Lee
Korea University
Gyudo Lee
Korea University
Ohwon Kwon
Korea Institute of Machinery and Materials

Nano Express

Keywords: polyaniline, nanoskein, convertible nanoprobe, glucose sensing, redox states

Posted Date: September 3rd, 2020

DOI: https://doi.org/10.21203/rs.3.rs-70453/v1

Version of Record: A version of this preprint was published on November 13th, 2020. See the published version at https://doi.org/10.1186/s11671-020-03446-2.

Abstract

Polyaniline nanoskein (PANS), which have polyaniline nanofibers, is developed. PANS is formulated via sequential extracting, heating, and swelling processes. The compositions of PANS have been analyzed using X-ray photoelectron spectroscopy, Fourier transform infrared spectroscopy, thermogravimetric analysis, and Brunauer-Emmett-Teller analysis, and the results of which indicate that PANS is composed of solely organic materials. Moreover, PANS have been shown convertible absorbance characteristics according to surrounding acidic environments, and using these characteristics, the possibility of PANS for sensing of surrounding redox states changes is presented.

1. Introduction

Flower-shaped inorganic structures have been used for applications for catalysis [1, 2], biosensors [3, 4], and theragnostic agents [5]. There are some synthetic strategies for generating these complex structures. The synthesis using template is the first approach, for instance, liposome have been used as a soft template to guide the formation of dendritic Pt sheets [6, 7]. The second approach is based on the phenomenon of oriented attachment of primary nanoparticles when surfaces with similar atomic arrangements approach each other. The synthesis of dendritic PtRu nanoparticles form faceted PtRu primary nanoparticles was based on this principle [8]. The third approach relies on the use of specific capping agents or surfactants to induce anisotropic growth of inorganic materials. The syntheses of Pt and Au multi-pods in the presence of poly(vinylpyrrolidone) or cetyltrimethylammonium bromide are examples [9, 10]. In addition, after the first approach by Ge et al. [2], organic-inorganic hybrid flower-shaped structures have been also intensively studied. In the process of synthesis for hybrid flower-shaped structures, the combinations of various proteins (e.g. enzymes [11] and DNA [12]) and metal ions (e.g. Cu [13], Ca [14, 15], and Mn [16]) have been used. In recent years, there were studies that synthesis of flower-shaped structures based on polyaniline (PAni) using strong acid doping [17], and polyurethane nanofiber [18].

In this study, we report a method for formulating organic flower-shaped structures, which is mostly composed of PAni, and its properties of matter. PAni, which is a representative conducting polymer, is used as an organic component in this study. PAni is well known for convertible optical properties due to its unique doping/dedoping or oxidation/reduction processes [19]. Using this phenomenon, our research group has reported that PAni-mediated nanostructures can be used as photo-thermal agents [20] and redox sensing probes [21, 22] for biomedical applications.

We give a name to flower-shaped PAni particles as PAni nanoskein (PANS) because the shape of PANS seems like a ball of yarn, which is composed of PAni nanofibers. Moreover, as-synthesized PAni appears to intrinsically form fibrillar and linear molecular structure such as thread. PANS was synthesized when we added benzyl ether (BE) to N-metyl-2-pyrrolidone (NMP) solution containing PAni, and this mixture was passed through heating and purification processes (Fig. 1a). And then, changes of surrounding redox states were sensed based on color change of PANS, where optical properties are converted (Fig. 1b).

2. Materials And Methods

2.1. Materials

Polyaniline (PAni) Mw ~ 5,000, benzyl ether (BE), glucose oxidase (GOx, from Aspergillus Niger, 145,200 units/g), and D-(+)-glucose were purchased from Sigma-Aldrich (St. Louis, MO, USA). N-Methyl-2-Pyrrolidone (NMP) and ethanol (EtOH) were purchased from Dae-jung, KOREA. Dulbecco's phosphate buffered saline (DPBS) was purchased from Welgene, Korea, buffer solution (pH 4) was purchased from Samchun, Korea. All other chemicals and reagents were analytical grade. Ultrapure deionized water (DW) was used for all the synthetic processes.

2.2. Synthesis of polyaniline nanoskein (PANS)

The synthetic process of immaculate product was as follows: PAni (250 mg) was dissolved in NMP (20 mL), and then BE (40 mL) was added. The mixture was preheated to 200 °C for 1 hour and heated to 300 °C for 30 minutes. The reactant was cooled in room temperature for 3 hours. The resultant solution was washed with excess of EtOH, and separated the precipitant by centrifuging at 3,000 rpm for 10 minutes. Then, the solution was re-dispersed in EtOH. Next, the solution dissolved in EtOH was dialyzed using dialysis membrane (MWCO: 3,500 Spectra/Por® 6, SPECTRUM® LABORATORIES, Rancho Dominguez, CA, USA) for 24 hours. After dialysis, the solution was centrifuged at 15,000 rpm for 30 minutes. The precipitant was re-dissolved in 30 mL of DW. The final concentration of PANS was calculated as 8.33 mg/mL.

2.3. Characterization of PANS

The morphology of PANS was evaluated with a transmission electron microscopic (TEM, JEM-1011, JEOL Ltd, Japan), and scanning electron microscopic (SEM, JSM-6701F, JEOL Ltd, Japan) imaging. X-ray photoelectron spectra were recorded using a K-alpha system (Thermo Fisher Scientific, Waltham, MA, USA). Fourier transform infrared spectra (FT-IR Spectrum Two, Perkin Elmer, Waltham, MA, USA) analysis was performed to confirm the characteristic bands of the synthesized PANS and the size distribution of the PANS was analyzed by dynamic light scattering (ELS-Z, Otsuka electronics, Japan) method. Furthermore, the surface area and pore volume of PANS was measured by Brunauer–Emmett–Teller analyzer (Autosorb-iQ 2ST/MP, Quantachrome Instruments, Boyton Beach, FL, USA) and the weight quantity of PANS was analyzed with a thermogravimetiric analyzer (SDT-Q600, TA instrument, New Castle, DE, USA). Moreover, the absorbance of PANS was analyzed using UV-vis spectrophotometer (Optizen 2120UV, MECASYS Co., Korea).

2.4. Glucose sensing using PANS

First of all, concentration of GOx was adjusted into 15 mg/mL using DPBS, and glucose was diluted with pH 4 buffer solution. The resultant concentration of glucose was set at 40, 20, 10, 5, and 1 mg/mL, respectively. And then, 1 mL of PANS (1.67 mg/mL) was mixed with 20 μL of GOx (15 mg/mL) and 80 μL of glucose (40, 20, 10, 5, and 1 mg/mL, respectively). The final concentrations of glucose in mixed

solutions were calculated as 2.91, 1.45, 0.73, 0.36, and 0.07 mg/mL, respectively. The absorbance of PANS with GOx and glucose was analyzed using UV-vis spectrophotometer (Optizen 2120UV, MECASYS Co., Korea).

3. Results And Discussion

The morphology of PANS was confirmed by transmission electron microscopic (TEM) and scanning electron microscopic (SEM) images as shown in Fig. 2. PANS exhibited spherical shape with hierarchical structures. In the synthetic process of PANS, first, PAni was dissolved into NMP, and then, BE was added to the PAni/NMP solution. Because of the solubility difference for PAni between NMP and BE, PAni was extracted into the mixture, so this process was referred as the ‘extracting’ process. After the extracting process, PAni appeared fibrillar shape, and this shape may be generated due to intermolecular proximity between PAni molecules (the first row in Fig. 2 and see also Fig. S1 in Supporting Information). After that, the mixture was heated sequentially at 200 °C for an hour and 300 °C for 30 minutes (‘heating’ process). The NMP has boiling point at about 203 °C, so PAni was existed in BE after the heating process. After the heating process, PAni was more nucleated than in the extracting process, and the shape of PANS was roundish. Moreover, the surface of PANS started to wrinkle, but many PANS particles were aggregated (the second row in Fig. 2 and see also Fig. S1 in Supporting Information). Subsequently, PANS was washed as well as swelled using ethanol (EtOH) (the third row in Fig. 2 and see also Fig. S1 in Supporting Information). After the swelling process, EtOH would be inserted between PAni molecules, so intermolecular distance also would be increased. Accordingly, PANS was existed at individual particles, and also had a hierarchical structure. To confirm the ideal condition of formulation of PNAS, the concentration of PAni was also controlled (Fig. S2 in Supporting Information). TEM images analysis according to feeding amount of PAni at each synthetic process (i.e. extracting, heating, and swelling process) was also conducted, and as feeding amount of PAni was decreased (from 50.0 mg/mL to 12.5 mg/mL), PANS was formulated much sparser. Moreover, the hierarchical structure of PANS was certainly confirmed via a 90°-tilted SEM image at feeding amount of PAni at 50 mg/mL (Fig. S3 in Supporting Information). For the detailed studies of formulating mechanism of PANS, solubility test of PAni was preferentially conducted (Fig. S4 in Supporting Information). PAni was known as hydrophobic and dissolved in a water-miscible polar aprotic solvent such as NMP [21]. The fibrillar shape of PAni was observed when PAni was dissolved in NMP. On the other hand, PAni in BE and EtOH had more aggregated and larger size than in NMP, furthermore, PAni in EtOH might be sparsely interacted with each PAni molecules. The solubility tests of PAni using measurements of absorbance spectra were also conducted, EtOH was shown the best solubility among the EtOH, BE, and deionized water (DW). The bare PAni molecules scarcely dissolved in DW. Moreover, another condition experiments were also conducted according to molecular weight (Mw) of PAni (Fig. S5 in Supporting Information). In the case of Mw 5 k Da, PANS exhibited more skein-like structures than other conditions (i.e. Mw 10 k Da and 50 k Da). In other cases, PAni did not nucleate such as Mw 5 k Da, and this phenomenon may be solubility differences to NMP for PAni. In another words, as the Mw of PAni is increased, PAni tends to insoluble in NMP, thereby PAni would not exist PAni nanofibers in NMP. As a result, sufficient PAni nanofibers were not

existed, so skein-like structures of PANS also would not be formulated. From these results, formulation of PANS is hypothesized as follows: 1) bare PAni does not dissolve in DW at all; 2) PAni have the best solubility in NMP; 3) PAni in NMP was extracted by addition of BE via solubility difference; 4) the NMP was vaporized by heating process from PAni/(NMP and BE) mixture; 5) the resultant solution is washed by EtOH, and the EtOH is inserted between PAni molecules; 6) PANS particles are swelled and well-dispersed in DW.

To study the characteristics of PANS, first of all, high resolution TEM (HRTEM) imaging analysis was conducted (Fig. 3a). PANS had morphology for a ball of yarn, which was composed of many PAni nanofibers. To verify the molecular structure of PANS, X-ray photoelectron spectroscopic (XPS) analysis for bare PAni (bPAni) and PANS were conducted (Fig. 3b and see also Fig. S6 in Supporting Information). The C1s core level spectra can be deconvoluted in four peaks: C = O/C-O at 286.7 eV (1), C = N+/C-Cl at 285.8 eV (2), C-N/C = N at 285.0 eV (3), and C-C/C-H at 284.4 eV (4), respectively. Deconvolution of C1s was based on data reported earlier by Golczak et al [23]. In particular, the changes of distributions for (3) and (4) were remarkable, and these result mean that nitrogen portion was increased in PANS. This phenomenon may be attributed to existence of NMP in PANS structures, and this NMP molecules affects interactions between PAni molecules for formulation of PANS. To further investigate for molecular structure of PANS, Fourier transform infrared (FTIR) spectra for bPAni and PANS were also analyzed (Fig. 3c and see also Fig. S7 in Supporting Information). The peaks at 1,290 cm^{-1} (aromatic C-N stretching), 1,490 cm^{-1} (C = C and C = N stretching of benzenoid ring), and 1,590 cm^{-1} (C = C and C = N stretching of quinoid ring) were confirmed in both of cases for bPAni and PANS. The specific peaks of PANS at 1,670 cm^{-1} (asterisk in Fig. 3c) might be attributed to tertiary amine in NMP, and this peak was also observed in FTIR spectrum of NMP (Fig. S7 in Supporting Information). Thermogravimetric analysis (TGA) results of bPAni and PANS reveal that PANS was composed of not only PAni but also other molecules (Fig. 3d). The degradation of bPAni was observed at about 350 °C, however, the degradation point of PANS was observed at about 200 °C, which coincides with boiling point of NMP. From XPS to TGA results (Fig. 3b-d) reveal that PANS was not only consist of pure PAni, but also consist of PAni and other organic compound such as NMP. Additionally, surface area and pore volume of PANS were determined by Brunauer-Emmett-Teller (BET) analysis (Fig. 3e), and PANS had 9.486 ± 0.728 m^2/g of surface area and 0.044 ± 0.004 cm^3/g of pore volume. (c.f. 6.358 ± 0.682 m^2/g of surface area and 0.019 ± 0.001 cm^3/g of pore volume for bPAni, respectively.) These results mean that PANS is more porous with high surface-to-volume ratio than bare PAni. The distribution of hydrodynamic diameter of PANS exhibited 799 ± 85 nm in an aqueous solution (Fig. 3f). These results in Fig. 3 show that PANS is solely composed of organic compounds (PAni and NMP) with hierarchical structures.

To investigate the possibility of PANS as convertible optical probes, color changes of PANS were analyzed using absorbance spectra. The changes of absorbance properties of PAni structures, such as nanoparticles, films, and sheets are well-known as varying its doping/dedoping states. The doping/dedoping states of PAni can be adjusted by various dopants, such as strong acids, Lewis acids, transitional metals, and alkali ions [24, 25]. PANS also exhibited those of properties according to changes

of surrounding pH values (Fig. 4). At low pH (< pH 2), PANS transitioned to an emeraldine salt (ES, green color) state, as indicated by the presence of the π-π* transition of the benzenoid rings as well as polaron bands transitions at about 480 and 800–900 nm, respectively [26]. With increasing pH value, the peaks at 480 and 800–900 nm are gradually decreased in absorbance, and a strong absorbance peak at about 680 nm is observed. The absorbance peak at 680 nm is attributed to excitation from highest occupied molecular orbital of the three-ring bezenoid part of the PAni to the lowest unoccupied molecular orbital of the localized quinoid ring and the two surrounding imine nitrogens in the emeraldine base (EB) state of the PAni [27]. To distinguish more accurately between ES and EB state of PANS, the absorbance ratio ($\lambda_{680}/\lambda_{480}$), was calculated at representative wavelength positions of peaks at EB and ES states of PANS, respectively (Fig. 4c). As the pH value decreased from 10 to 4, the absorbance ratio maintained at nearly 1.06, and it decreased dramatically to nearly 0.88 at pH values from 4 to 1. These results indicate that spectral changes of PANS can be used to sense the specific changes of redox state by changes of surrounding environments.

To investigate the sensing capability of PANS for specific changes of redox state by changes of surrounding environments, glucose and GOx were selected as representative candidates. As increasing the concentrations of glucose from 0.00 to 2.91 mg/mL, the color of PANS solutions changed from blue to green color (Fig. 5a). The absorbance spectra of PANS were also analyzed (Fig. 5b), but shape changes in spectra were less than those in experiments with pH changes as shown in Fig. 4. However, the values of absorbance ratio ($\lambda_{680}/\lambda_{480}$) was formed between 0.98 and 0.86, and this result indicate that PANS is existed at intermediated state ($\lambda_{680}/\lambda_{480}$ = 0.98) and ES state ($\lambda_{680}/\lambda_{480}$ = 0.86) as shown in Fig. 5c. The reaction between glucose and GOx is representative redox reaction, and this reaction is well-known for producing hydrogen peroxide resulting in hydrogen ions and electrons. These results indicate that PANS can be doped with hydrogen ions and electrons. As a result, the π–π* transition of the benzenoid ring is observed in absorbance spectra through the formation of shoulder at 480 nm.

4. Conclusion

In summary, formulation of skein-shaped PANS, which is composed of PAni fibers has been achieved, and the formulating mechanism has been also proposed. The synthetic process of PANS contains sequential extracting, heating, and swelling processes. The compositions of PANS have been analyzed, and PANS have been composed of solely organic materials. Moreover, possibilities of PANS as convertible optical probes for sensing of surrounding redox states changes were confirmed via change of pH values and combination of glucose and GOx. The present study sheds light on the synthesis of new class of 3D shaped nanostructures as well as nanobiosensors for sensing of surrounding redox state changes.

Declarations

Availability of data and materials

All data generated or analyzed during this study are included in this published article.

Competing interests

The authors declare that they have no competing interests.

Funding

This work was supported by the projects of Korea Institute of Machinery and Materials (KIMM) (NK226D). This research was also supported by Basic Science Research Program through the National Research Foundation of Korea (NRF) funded by the Ministry of Education (2017R1A6A3A11034311) and by Korea University Grant.

Author’s contributions

All the authors equally participated at all the research levels. The authors read and approved the final manuscript.

Acknowledgements

Not applicable

References

1. Mohanty A, Garg N, Jin R (2010) A universal approach to the synthesis of noble metal nanodendrites and their catalytic properties, Angew. Chemie - Int Ed 49:4962–4966. https://doi.org/10.1002/anie.201000902
2. Ge J, Lei J, Zare RN (2012) Protein-inorganic hybrid nanoflowers. Nat Nanotechnol 7:428–432. https://doi.org/10.1038/nnano.2012.80
3. Xie J, Zhang Q, Lee JY, Wang DIC (2008) The Synthesis of SERS-Active Gold Nanoflower Tags for In Vivo Applications. ACS Nano 2:2473–2480. https://doi.org/10.1021/nn800442q
4. Jia W, Su L, Lei Y (2011) Pt nanoflower/polyaniline composite nanofibers based urea biosensor. Biosens Bioelectron 30:158–164. https://doi.org/https://doi.org/10.1016/j.bios.2011.09.006
5. Huang J, Guo M, Ke H, Zong C, Ren B, Liu G, Shen H, Ma Y, Wang X, Zhang H, Deng Z, Chen H, Zhang Z (2015) Rational Design and Synthesis of γFe2O3@Au Magnetic Gold Nanoflowers for Efficient Cancer Theranostics. Adv Mater 27:5049–5056. https://doi.org/10.1002/adma.201501942
6. Song Y, Yang Y, Medforth CJ, Pereira E, Singh AK, Xu H, Jiang Y, Brinker CJ, van Swol F, Shelnutt JA (2004) Controlled Synthesis of 2-D and 3-D Dendritic Platinum Nanostructures. J Am Chem Soc

126:635–645. https://doi.org/10.1021/ja037474t

7. Song Y, Steen WA, Peña D, Jiang Y-B, Medforth CJ, Huo Q, Pincus JL, Qiu Y, Sasaki DY, Miller JE, Shelnutt JA (2006) Foamlike Nanostructures Created from Dendritic Platinum Sheets on Liposomes. Chem Mater 18:2335–2346. https://doi.org/10.1021/cm060384d
8. Teng X, Maksimuk S, Frommer S, Yang H (2007) Three-Dimensional PtRu Nanostructures. Chem Mater 19:36–41. https://doi.org/10.1021/cm061979b
9. Hao E, Bailey RC, Schatz GC, Hupp JT, Li S (2004) Synthesis and Optical Properties of “Branched” Gold Nanocrystals. Nano Lett 4:327–330. https://doi.org/10.1021/nl0351542
10. Nehl CL, Liao H, Hafner JH (2006) Optical Properties of Star-Shaped Gold Nanoparticles. Nano Lett 6:683–688. https://doi.org/10.1021/nl052409y
11. Sun J, Ge J, Liu W, Lan M, Zhang H, Wang P, Wang Y, Niu Z (2014) Multi-enzyme co-embedded organic–inorganic hybrid nanoflowers: synthesis and application as a colorimetric sensor. Nanoscale 6:255–262. https://doi.org/10.1039/C3NR04425D
12. Hu R, Zhang X, Zhao Z, Zhu G, Chen T, Fu T, Tan W (2014) DNA Nanoflowers for Multiplexed Cellular Imaging and Traceable Targeted Drug Delivery, Angew. Chemie Int Ed 53:5821–5826. https://doi.org/10.1002/anie.201400323
13. Lin Z, Xiao Y, Wang L, Yin Y, Zheng J, Yang H, Chen G (2014) Facile synthesis of enzyme–inorganic hybrid nanoflowers and their application as an immobilized trypsin reactor for highly efficient protein digestion. RSC Adv 4:13888–13891. https://doi.org/10.1039/C4RA00268G
14. Wang L-B, Wang Y-C, He R, Zhuang A, Wang X, Zeng J, Hou JG (2013) A New Nanobiocatalytic System Based on Allosteric Effect with Dramatically Enhanced Enzymatic Performance. J Am Chem Soc 135:1272–1275. https://doi.org/10.1021/ja3120136
15. Wang X, Shi J, Li Z, Zhang S, Wu H, Jiang Z, Yang C, Tian C (2014) Facile One-Pot Preparation of Chitosan/Calcium Pyrophosphate Hybrid Microflowers. ACS Appl Mater Interfaces 6:14522–14532. https://doi.org/10.1021/am503787h
16. Zhang Z, Zhang Y, Song R, Wang M, Yan F, He L, Feng X, Fang S, Zhao J, Zhang H (2015) Manganese(II) phosphate nanoflowers as electrochemical biosensors for the high-sensitivity detection of ractopamine. Sensors Actuators B Chem 211:310–317. https://doi.org/https://doi.org/10.1016/j.snb.2015.01.106
17. Noby H, El-Shazly AH, Elkady MF, Ohshima M (2019) Strong acid doping for the preparation of conductive polyaniline nanoflowers, nanotubes, and nanofibers. Polymer 182:121848. https://doi.org/https://doi.org/10.1016/j.polymer.2019.121848
18. Khosrozadeh A, Darabi MA, Wang Q, Xing M (2017) Polyaniline nanoflowers grown on vibration-isolator-mimetic polyurethane nanofibers for flexible supercapacitors with prolonged cycle life. J Mater Chem A 5:7933–7943. https://doi.org/10.1039/C7TA00591A
19. Hong Y, Hwang S, Yoon DS, Yang J (2015) Scattering analysis of single polyaniline nanoparticles for acidic environmental sensing. Sensors Actuators B Chem 218:31–36. https://doi.org/10.1016/j.snb.2015.04.098

20. Yang J, Choi J, Bang D, Kim E, Lim EK, Park H, Suh JS, Lee K, Yoo KH, Kim EK, Huh YM, Haam S (2011) Convertible organic nanoparticles for near-infrared photothermal ablation of cancer cells, Angew. Chemie - Int Ed 50:441–444. https://doi.org/10.1002/anie.201005075
21. Choi J, Hong Y, Lee E, Kim M-H, Yoon DS, Suh J, Huh Y, Haam S, Yang J (2013) Redox-sensitive colorimetric polyaniline nanoprobes synthesized by a solvent-shift process. Nano Res 6:356–364. https://doi.org/10.1007/s12274-013-0312-z
22. Hong Y, Hwang S, Heo D, Kim B, Ku M, Lee E, Haam S, Yoon DS, Yang J, Suh J-S (2015) A magnetic polyaniline nanohybrid for MR imaging and redox sensing of cancer cells. Nanoscale 7:1661–1666. https://doi.org/10.1039/C4NR06340F
23. Golczak S, Kanciurzewska A, Fahlman M, Langer K, Langer JJ (2008) Comparative XPS surface study of polyaniline thin films. Solid State Ionics 179:2234–2239. https://doi.org/https://doi.org/10.1016/j.ssi.2008.08.004
24. Gizdavic-Nikolaidis M, Travas-Sejdic J, Bowmaker GA, Cooney RP, Kilmartin PA (2004) Conducting polymers as free radical scavengers. Synth Met 140:225–232. https://doi.org/https://doi.org/10.1016/S0379-6779(03)00372-2
25. Dimitriev OP (2004) Doping of Polyaniline by Transition-Metal Salts. Macromolecules 37:3388–3395. https://doi.org/10.1021/ma035677w
26. Huang WS, MacDiarmid AG, Optical properties of polyaniline, Polymer (Guildf). 34 (1993) 1833–1845. https://doi.org/10.1016/0032-3861(93)90424-9
27. Huang J, Kaner RB, The intrinsic nanofibrillar morphology of polyaniline, Chem Commun (2006) 367–376. https://doi.org/10.1039/B510956F

Figures

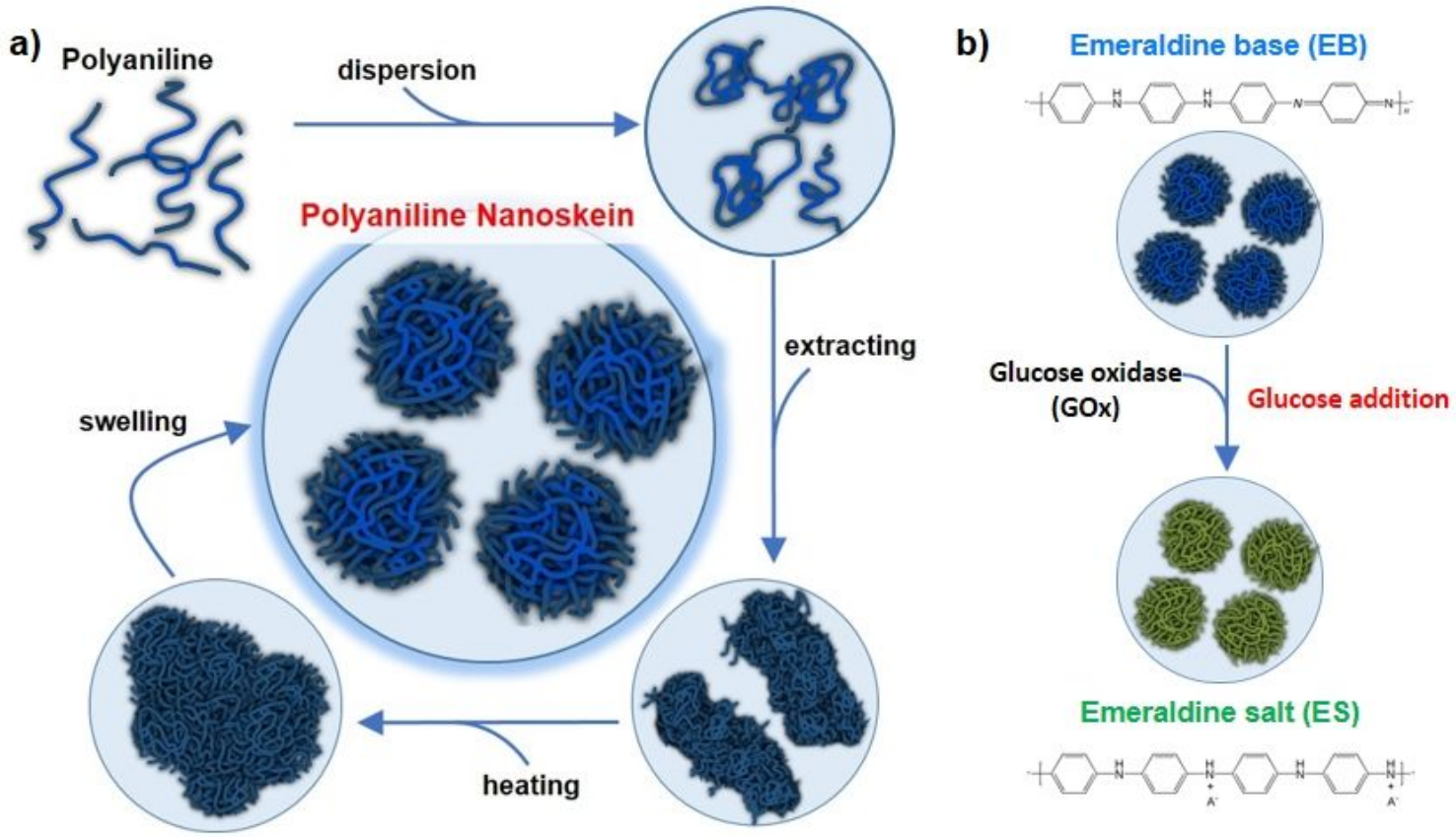

Figure 1

a) The synthetic process of polyaniline nanoskein (PANS). b) Glucose sensing process using PANS.

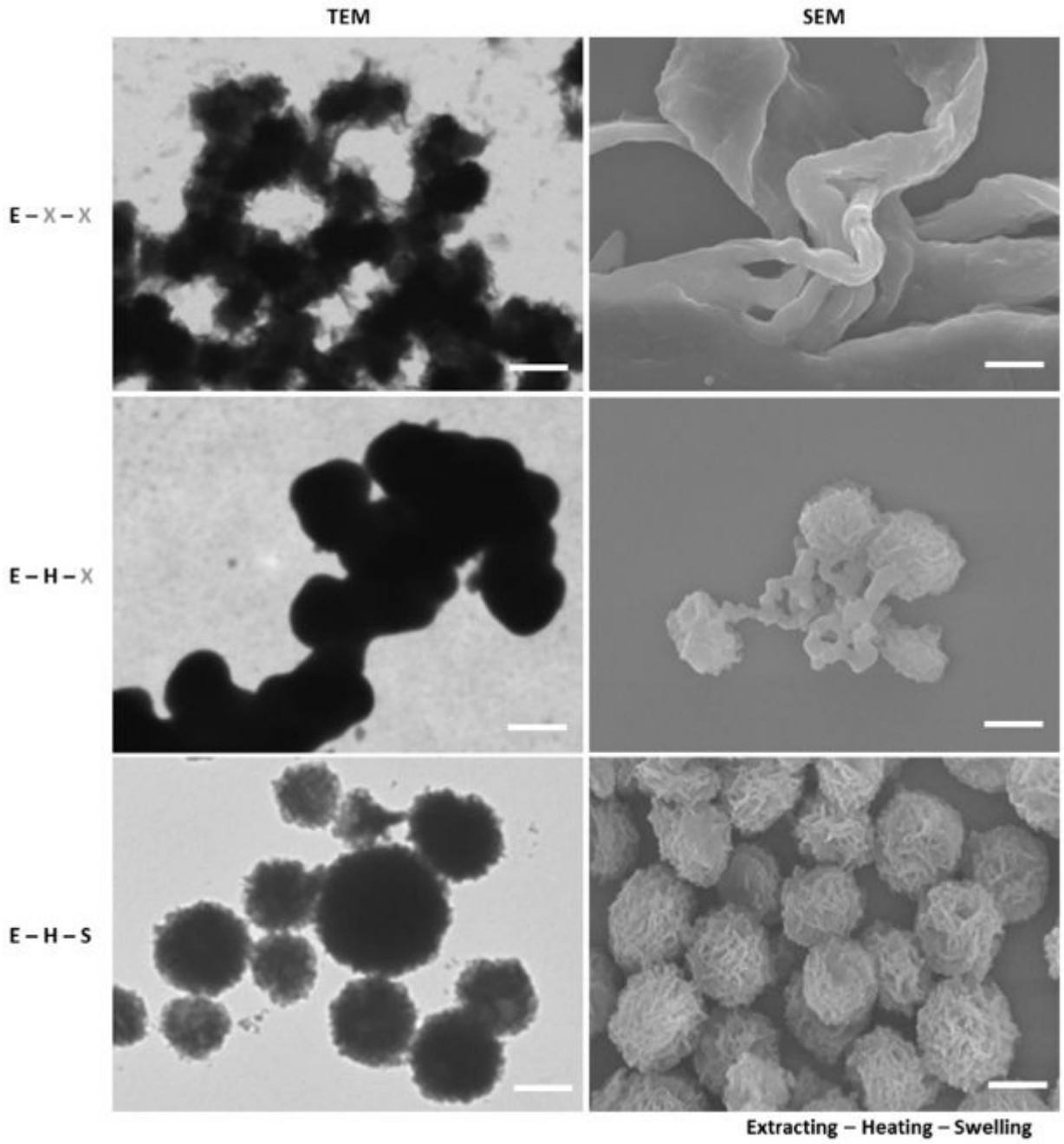

Figure 2

Morphology of PANS via transmission electron microscopic (TEM, left) and scanning electron microscopic (SEM, right) imaging. Alphabetic characters represent sequential synthetic processes of PANS; (E): extracting reactant with BE, (H): heating sequentially the reactant at 200°C and 300°C, and (S): swelling the reactant using EtOH. Note that (X): no treatment. Scale bars are 500 nm.

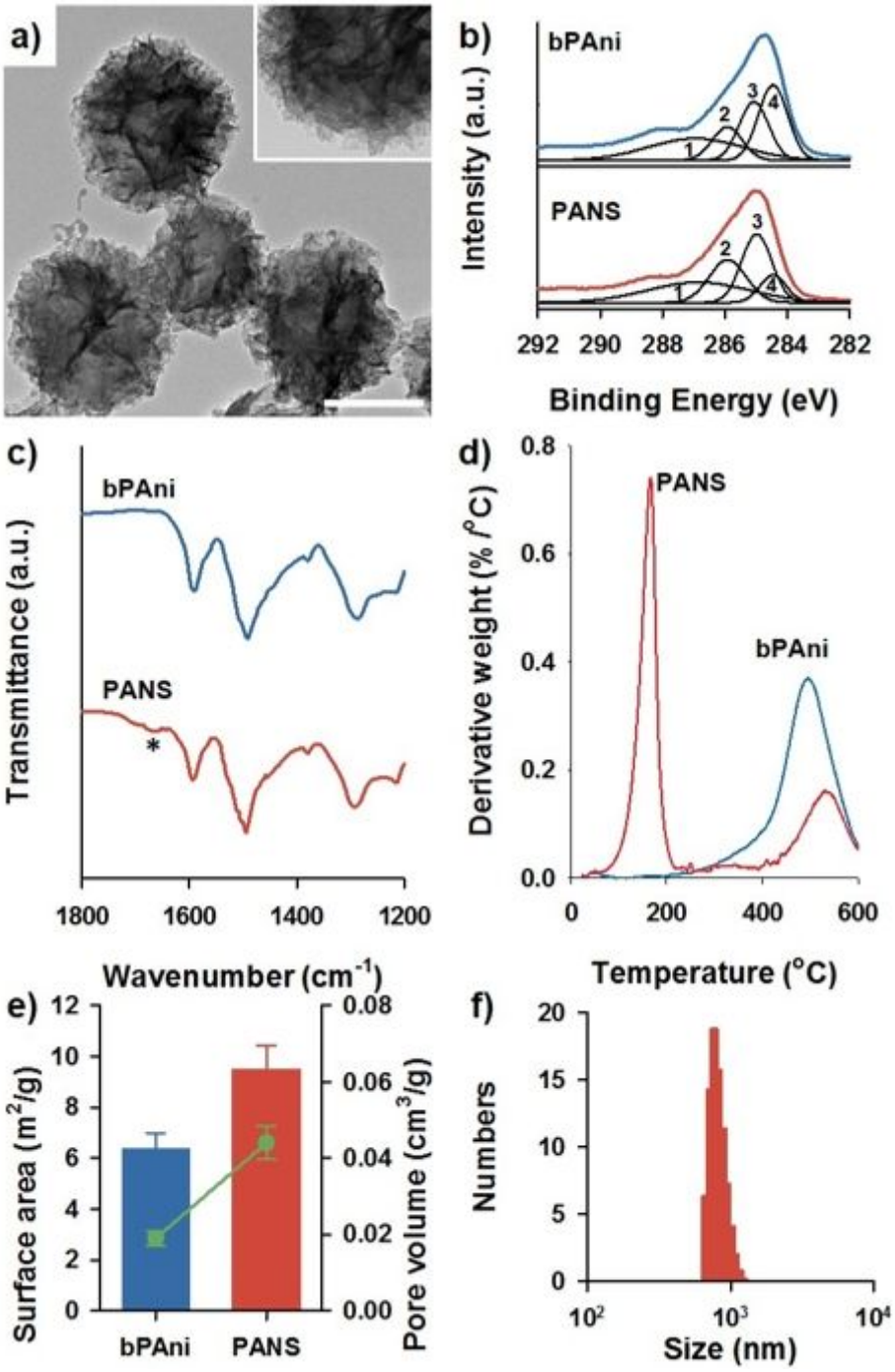

Figure 3

a) High resolution trasmission electron microscopic (HRTEM) images of PANS. Scale bar is 100 nm, and inset is a high magnification image. b) XPS C1s spectra of bare polyaniline (bPAni) (upper) and PANS (lower). 1: C=O/C-O, 2: C-N+/C=N+, 3: C-N/C=N, 4: C-C/C-H. c) FTIR spectra of bPAni (upper) and PANS (lower). An asterisk represents a interesting peak described in more detail in the text. d) Thermogravimetric analysis (TGA) of bPAni (upper) and PANS (lower). e) Surface area (bar) and pore volume (line and scatter) of bPAni and PANS using Brunauer–Emmett–Teller (BET) analysis. f) Size distribution of PANS via dynamic light scattering (DLS) method.

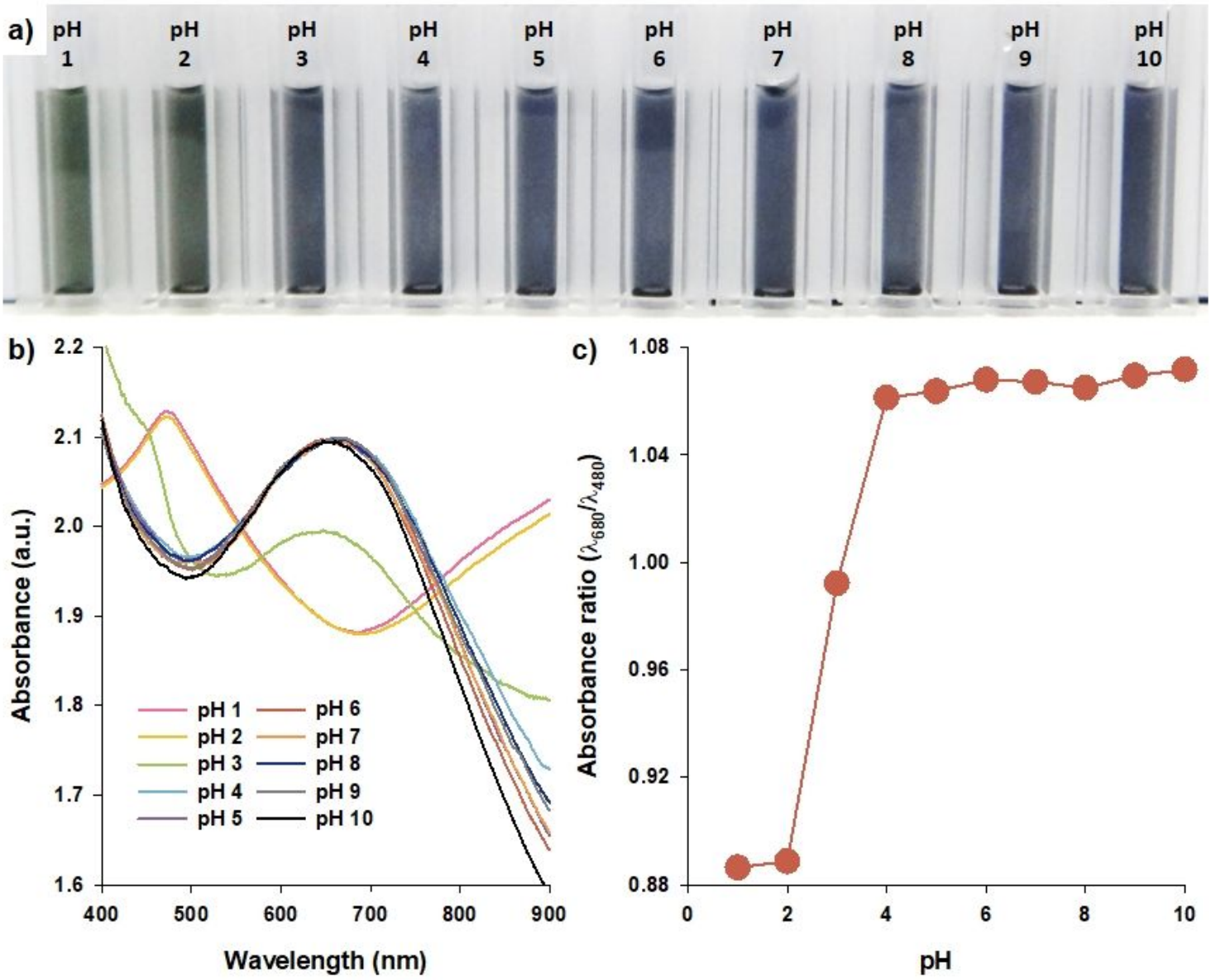

Figure 4

a) A photograph, b) absorbance spectra, and c) absorbance ratio for specific wavelengths representative wavelength for EB (at 680 nm) and ES (at 480 nm) states of PANS solutions in indicated pH conditions.

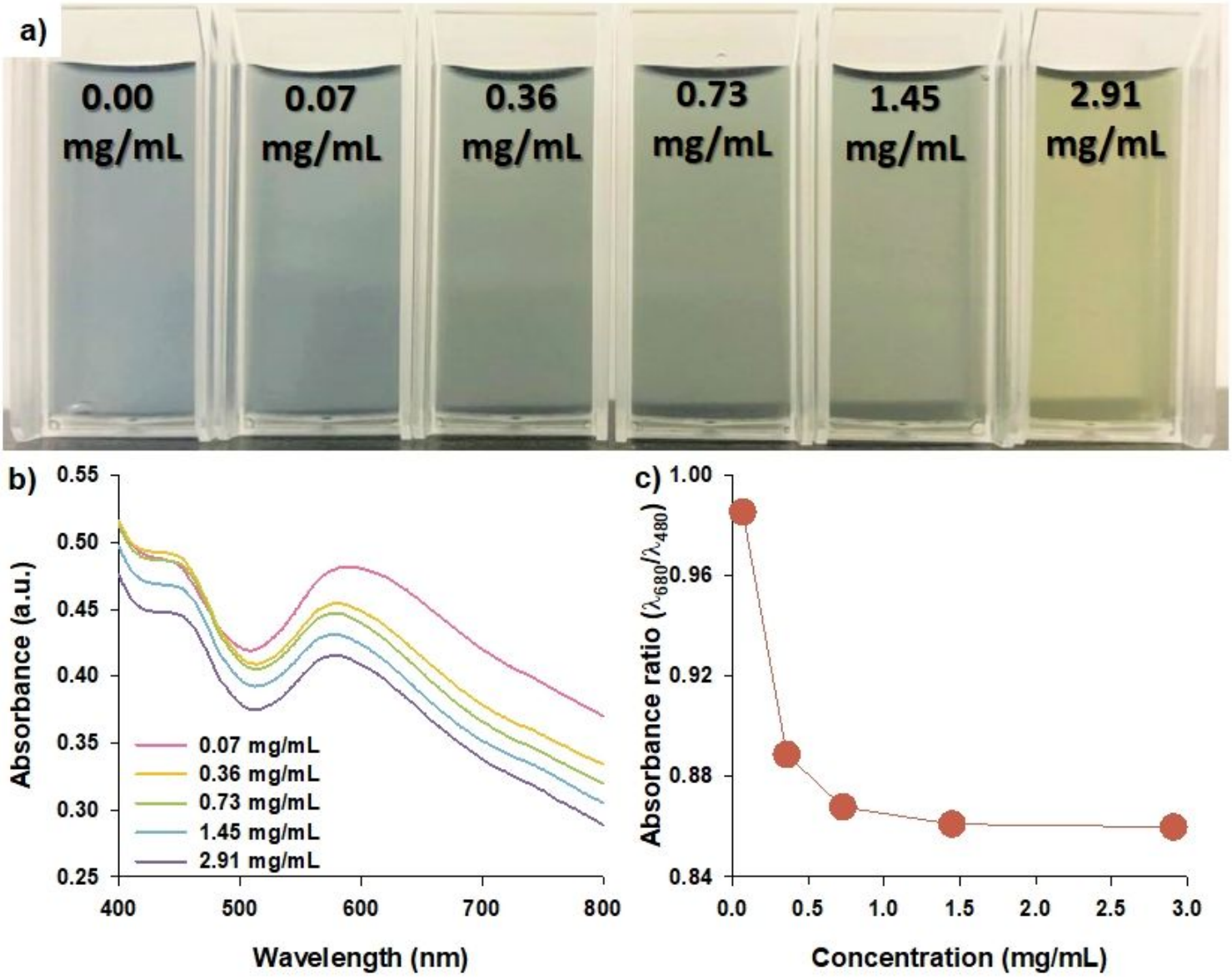

Figure 5

a) A photograph, b) absorbance spectra, and c) absorbance ratio for specific wavelengths representative wavelength for EB (at 680 nm) and ES (at 480 nm) states of PANS solutions with indicated glucose concentrations.

Supplementary Files

This is a list of supplementary files associated with this preprint. Click to download.

- 003.SupportingInformation.docx